

# Multiparameter estimation for the superresolution of two incoherent sources

Antonin Grateau<sup>1</sup>, Alexander Boeschoten<sup>1</sup>, Tanguy Favin-Lévéque<sup>1</sup>, Isael Herrera<sup>1</sup>, and Nicolas Treps<sup>1\*</sup>

<sup>1</sup>*Laboratoire Kastler Brossel, Sorbonne Université, ENS-Université PSL,  
CNRS, Collège de France, 4 Place Jussieu, F-75252 Paris, France*

(Dated: January 22, 2026)

We experimentally demonstrate the simultaneous estimation of the three parameters characterizing a pair of incoherent optical sources in the sub-Rayleigh regime, enabling super-resolved scene characterization. Using spatial-mode demultiplexing (SPADE) with two demultiplexers—one deliberately shifted—we determine separations well below the diffraction limit and achieve sensitive joint estimation of separation, centroid, and relative brightness over a broad range of scene configurations in a single experimental setting. We benchmark our performance using Fisher-information-based Cramér–Rao bounds, and discuss the corresponding quantum limits. We investigate two complementary scenarios: a realistic case with slightly non-identical sources, and an idealized case of indistinguishable sources.

## I. INTRODUCTION

Imaging is the process of extracting information about a system or object from the light that it emits or scatters. It can therefore be formulated as a parameter estimation problem: one or more parameters – for example, the object’s position, its size, and its brightness – are encoded in the light, the carrier of information, and need to be estimated [1–8]. The detection of the light and estimation strategy of the parameter from the data constitute the measurement and determine the quality of the estimation and its fundamental limitations.

Conventionally, imaging employs a pixelized intensity measurement, also known as direct imaging (DI). However, for certain imaging tasks, DI has severe limitations and other measurement strategies should be employed. An important example is the estimation of the separation between two incoherent point sources, a single-parameter estimation problem. DI is limited by diffraction of the light on a finite aperture, and therefore unable to resolve objects when their overlap is considerably larger than the size of the point-spread function [9–12]. Evaluating this problem from a quantum metrology point of view, it becomes clear that this is not a fundamental limitation. In particular, Tsang *et al.* [13] showed that whereas in DI the information per photon vanishes at small separations, the quantum Cramér–Rao bound (QCRB), which sets the ultimate precision limit, remains finite and separation independent, even in the limit of zero separation. It was shown that an intensity measurement in the Hermite–Gauss (HG) mode basis, known as spatial mode demultiplexing (SPADE), achieves this bound.

This technique has been experimentally implemented, and the superiority of SPADE over DI is verified in several experiments using different techniques [14–21]. However, realistic imaging scenarios are inherently multiparametric. For instance, the image of two point sources is defined by their separation, their centroid position, and

their relative intensities. These parameters are simultaneously encoded in the optical field and are not independent [22, 23]. Therefore, the ultimate precision limits and the optimal measurement strategies require the framework of multiparameter estimation theory [24–26]. From this perspective, multiparameter estimation can be viewed as the step between single-parameter estimation and full image reconstruction, thereby enabling super-resolved imaging of simple scenes [27–33].

The joint estimation of centroid and distance has been performed with different techniques, all based on SPADE [34, 35]. However, these experiments still assume the sources to have equal intensity. Recently, the simultaneous estimation of the intensity imbalance and separation, assuming a known barycenter, was performed [36], but the full three parameter estimation has only been done in the time domain and sequentially [37]. Indeed, the real challenge of multiparameter estimation lies not only in achieving high precision for a specific scene, but also in designing a measurement strategy that provides robust sensitivity over a wide range of possible scenes, without prior knowledge of the parameters to be estimated.

In this letter, we experimentally perform the simultaneous estimation of the separation, centroid, and intensity imbalance of two incoherent point sources over a broad range of parameter values. This is done in a single experimental setting, without adapting the measurement to the unknown scene. Our approach relies on two spatial demultiplexers (Multi-Plane Light Converters, MPLCs), with one deliberately shifted to enhance the information. This scheme is more robust and versatile than implementing the full set of optimal modes [23, 37], which are at the same time scene-dependent and challenging to realize in practice, and thus experimentally relevant. Importantly, our analysis highlights the subtleties that arise when moving from the ideal theoretical case to realistic experimental conditions, where the two sources are slightly different, and paves the way for practical applications.

In what follows, we first show how the dual-MPLC configuration enhances parameter sensitivity compared to a single-MPLC setup. We then present results for

\* [nicolas.treps@lkb.upmc.fr](mailto:nicolas.treps@lkb.upmc.fr)

experimental source configurations, and finally address the more fundamentally challenging scenario of indistinguishable sources, investigated using data obtained from a single light source.

## II. TWO MODE-BASIS APPROACH FOR MULTIPARAMETER ESTIMATION

Performing multiparameter estimation is not only about achieving good precision for a specific scene, but also about designing an experimental configuration that provides robust sensitivity over a wide range of possible scenes. In this work, rather than tailoring an optimal mode decomposition for a particular parameter set, we aim at a versatile measurement strategy that remains informative across the full parameter space. To this end, we introduce a dual-basis approach based on two commercial multi-plane light converters (MPLCs), which decompose the incoming field into two shifted Hermite–Gaussian mode bases.

It is well known that a single Hermite–Gaussian basis is insufficient to simultaneously estimate the source separation  $d$ , centroid  $c$ , and brightness imbalance  $p$ , due to the intrinsic symmetries of this basis. Previous work has shown that the unavoidable asymmetries of a practical MPLC can be exploited to access limited multiparameter information for equally bright sources [34]. However, this effect is weak and does not enable three-parameter estimation. We therefore use two mode bases: the first MPLC provides a practical Hermite–Gaussian mode decomposition, while the second MPLC is deliberately shifted laterally, resulting in a complementary mode basis. In practice, we use the first four horizontal modes of the first MPLC to extract most of the available information, and we include a single mode from the shifted MPLC to lift remaining degeneracies. This addition significantly improves robustness, reducing estimator bias and enhancing sensitivity across the parameter space.

To quantify the benefit of the dual-MPLC configuration, we compare its theoretical sensitivity to that of a single-MPLC setup using experimentally realistic conditions, including imperfect mode decomposition and source non-idealities. We construct estimators directly from experimentally measured calibration curves. By using either one or two sets of calibration curves, we can model distinguishable and indistinguishable sources, respectively. For each configuration, we compute the classical Fisher information matrix and the associated Cramér–Rao bounds (CRBs), assuming shot-noise-limited detection (see Supp. Mat.). These bounds provide a lower limit on the achievable standard deviation for each parameter  $\alpha \in \{d, c, p\}$ ,

$$\sigma_\alpha \geq \sigma_{\alpha, \text{CRB}} = \sqrt{(\mathcal{F}^{-1})_{\alpha\alpha}}. \quad (1)$$

We perform our simulations on an ensemble of scenes spanning the relevant parameter range at fixed total pho-

ton number. For each configuration (one versus two MPLCs) and for each scene, we compute the full Fisher information matrix and extract the marginal Cramér–Rao bounds on each parameter.

Fig. 1 presents plots of the CRBs for  $\sigma_d$ , as a function of the source separation  $d/w_0$ . In the Supp. Mat. we show similar plots associated with the parameters  $c$  and  $p$ . In solid line we show the mean value of  $\sigma_{d, \text{CRB}}$  and, to illustrate the dependence of the sensitivity on the true values of the scene, we show a shaded area containing 90% of the computed values of the CRB. The dual-MPLC configuration reduces the dependence on the three parameters, and also reduces the average value of the CRB compared to the one computed for the single-MPLC configuration. For the case of indistinguishable sources we included the averaged value of the QCRB, computed as in Ref. [22], we found a minimum difference of a factor of  $\sim 8$ , between the classical sensitivity of the 2-MPLC configuration and the QCRB.

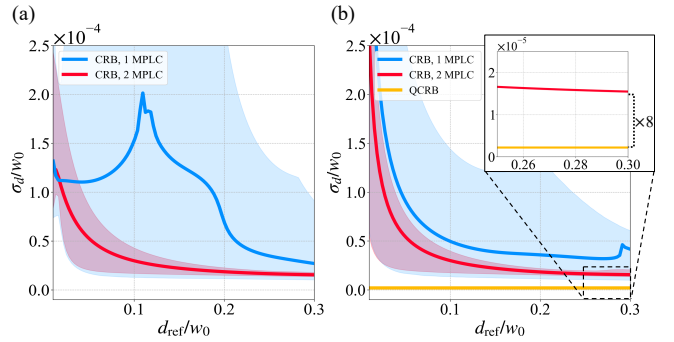


FIG. 1. Cramér–Rao bounds associated with  $d$ , for one and two MPLC configuration associated with (a) distinguishable and (b) indistinguishable sources. In solid lines we show the average precision on  $d$ . The corresponding shaded area is the region containing 90% of the computed values. We use an ensemble of scenes defined by  $d \in [0.01, 0.3]w_0$ ,  $c \in [-0.15, 0.15]w_0$  and  $p = 0.5$ , with  $N = 10^{11}$  signal photons. For indistinguishable sources we also show the quantum CRB, which exhibits nearly constant value of  $\approx 2.3 \times 10^{-6}$ .

## III. EXPERIMENTAL SETUP

The experiment, Fig. 2(b), is performed using two independent, fiber-coupled continuous-wave (CW) lasers at 1550 nm to generate two incoherent light sources. Each guided mode is passed through an optical isolator, a polarization controller, and a fibered attenuator, allowing for independent tuning of polarization and optical power. Once collimated into free space, they form Gaussian beams with a waist of  $w_1 \simeq 1135 \mu\text{m}$ . Each beam is reflected by a mirror mounted on a motorized translation stage (MTS) with a minimum step size of 20 nm, enabling fine adjustment of transverse displacement and precise control over spatial separation at the beam splitter. The combined beams are projected through a Glan-

Thomson polarizer to ensure a common linear polarization, so that the obtained scene closely reproduces the image of two indistinguishable point light sources by an optical system with a Gaussian PSF. A telescope images and mode-matches the beams for optimal coupling into a demultiplexer (multiplane light converter, MPLC, PROTEUS-C from Cailabs) with waist  $w_0 \simeq 320 \mu\text{m}$  [38]. It effectively implements a unitary transformation from these modes to spatially separated Gaussian modes, each coupled into a distinct single-mode fiber for independent detection. The light is split so that half of it is sent to another MPLC, transversely shifted with respect to the first one.

We limit ourselves to the one-dimensional problem, as the two components of the separation vector,  $\mathbf{d} = (d_x, d_y)$ , can be treated independently: each affects different sets of modes (horizontal versus vertical). For the estimations, we use the first four horizontal modes of the first MPLC,  $\text{HG}_{00}$ ,  $\text{HG}_{10}$ ,  $\text{HG}_{20}$ , and  $\text{HG}_{30}$ , along with the  $\text{HG}_{10}$  mode of the second MPLC (also referred to as  $\text{HG}_{10}^{2\text{nd}}$ ). The corresponding intensities are measured simultaneously with photodiodes, while an additional detector records the total power of the scene.

#### IV. MULTIPARAMETER ESTIMATIONS

##### A. Pre-procedure: Alignment, Mode-Matching, and Calibration

The experimental procedure begins with mode-matching the two sources to the first demultiplexer by

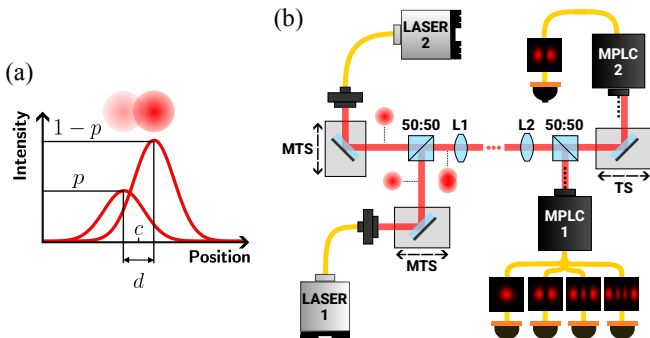


FIG. 2. (a) The 1D profile of two Gaussian beams with the same waist  $w_0$ , separated by a distance  $d$  and centered at  $c$  (with respect to the first MPLC origin). The brightness imbalance is characterized by the parameter  $p$ , so that the triplet  $\boldsymbol{\theta} = (d, c, p)^\top$  fully defines the scene. (b) Conceptual scheme of the setup. The left part corresponds to source generation, where motorized translation stages (MTS) are used to tune the positions of the two sources and change the scene. The brightness imbalance is controlled by adjusting the power in each source path via attenuators. The light is propagated through a telescope for mode-matching and then detected by the two demultiplexers, with one deliberately transversely shifted relative to the other (right part).

adjusting the telescope lens ratios to minimize the MPLC outputs corresponding to the  $\text{HG}_{20}$  and  $\text{HG}_{02}$  modes, which are sensitive to deviations of the source waist from the demultiplexer's intrinsic waist; this adjustment is done once and then kept fixed. Coarse alignment of both sources is achieved by maximizing the  $\text{HG}_{00}$  mode, while the  $\text{HG}_{10}$  and  $\text{HG}_{01}$  modes, highly sensitive to tilt and misalignment relative to the demultiplexer origin, are minimized for fine tuning.

Being a twin of the first MPLC with identical waist  $w_0$ , the second device operates under the same telescope and mode-matching conditions optimized for the first, and is aligned to the sources using the same strategy with  $\text{HG}_{00}^{2\text{nd}}$ ,  $\text{HG}_{10}^{2\text{nd}}$  and  $\text{HG}_{01}^{2\text{nd}}$ . It is then transversely shifted by an amount  $x_s = 0.3w_0$  using a linear translation stage, so that part of the light is measured in a different mode basis.

Calibration is performed by moving each source individually along the horizontal axis of the transverse plane using motorized stages, while recording all outputs at each position. This step characterizes the system's actual response and captures experimental imperfections such as misalignment, mode-matching errors, crosstalk, and deviations from an ideal Gaussian spatial profile. By normalizing this data with the total power and fitting it with a high-order polynomial, we obtain the fraction of intensity as a function of the source position:  $I_{i,j}(x_j)$ , where  $i \in \{0, 1, 2, 3, 4\}$  denotes the mode and  $j \in \{1, 2\}$  denotes the source. Note that, in theory, the two sources—being identical—should exhibit the same response. In practice, however,  $I_{i,1} \neq I_{i,2}$ ; this difference is quantified by a visibility of 99% between the two beams. When both sources are on, and since the light is incoherent, the fraction of intensity in mode  $i$  is given by the sum of the contributions from the two sources:

$$\mu_i(\boldsymbol{\theta}) = p I_{i,1} \left( c - \frac{d}{2} \right) + (1 - p) I_{i,2} \left( c + \frac{d}{2} \right). \quad (2)$$

Here  $\boldsymbol{\theta} = (d, c, p)^\top$  denotes the triplet of parameters that fully defines a scene (see Fig. 2(a)). We explore sub-Rayleigh separations and centroids, and three different imbalances – from equally bright sources to nearly ten times brighter – as summarized in Table I. The range of parameters is chosen to demonstrate that, with one experimental configuration, we can achieve simultaneous estimation of all three parameters with high accuracy and sensitivity. All experiments are performed in a relatively high photon flux regime (tens of micro-watts). Note that given the linearity of the device, it would be straightforward to extend the results to lower flux levels, with lower sensitivity as the photon flux is much lower, thus this configuration is much less sensitive to experimental imperfections than we can assess here at high flux.

TABLE I. Ranges of parameters in the measurements. Each scene corresponds to one combination of the points listed for each parameter. Note that negative distances are used for the two slightly different sources as it produces a different scene.

Distinguishable sources (99% overlap)			
Parameter	Range	Step	Number of points
$d$	$[-0.15, 0.15]w_0$	$\approx 0.03w_0$	10
$c$	$[-0.07, 0.07]w_0$	$\approx 0.03w_0$	5
$p$	$\{0.1, 0.3, 0.5\}$	—	3
Indistinguishable sources			
Parameter	Range	Step	Number of points
$d$	$[0.05, 0.3]w_0$	$\approx 0.06w_0$	5
$c$	$[-0.07, 0.07]w_0$	$\approx 0.03w_0$	5
$p$	$\{0.1, 0.3, 0.5\}$	—	3

## B. Results with distinguishable sources

We generate measurement data by scanning the horizontal axis of the transverse plane with the two motors and varying the source powers (keeping the total flux fixed at approximately 300  $\mu\text{W}$ ).

In total,  $10 \times 5 \times 3 = 150$  distinct scenes are recorded. For each scene, the reference parameters are first determined by measuring each source individually using a quadrant detector and an auxiliary photodiode to record its position and power. Next, both sources are measured simultaneously for 0.01 s at a 10 kHz sampling rate, producing 100 temporal measurement points (time bins) per scene; these data are used for parameter estimation.

For a given time bin, we estimate our parameters from the measured fraction of intensities in all modes  $\mathbf{y} = (y_0, y_1, \dots, y_4)^\top$ , using a maximum likelihood estimator under the assumption of multivariate Gaussian noise, by minimizing the following loss function:

$$\ell(\boldsymbol{\theta}) = (\mathbf{y} - \boldsymbol{\mu}_{\boldsymbol{\theta}})^\top \boldsymbol{\Gamma}^{-1} (\mathbf{y} - \boldsymbol{\mu}_{\boldsymbol{\theta}}) \quad (3)$$

where  $\boldsymbol{\Gamma}$  is the covariance matrix of the observation  $\mathbf{y}$ , and  $\boldsymbol{\mu}_{\boldsymbol{\theta}} = (\mu_0(\boldsymbol{\theta}), \mu_1(\boldsymbol{\theta}), \dots, \mu_4(\boldsymbol{\theta}))^\top$  are the expected fractions of intensities for a given  $\boldsymbol{\theta}$ . We estimate  $\boldsymbol{\Gamma}$  from the ensemble of 100 time bins and then treat it as known when analyzing a single bin. The minimization of the above cost function with respect to  $\boldsymbol{\theta}$  is performed numerically using differential optimization scheme.

Since the estimation is performed for each time bin, we have access to statistical errors  $\sigma_\alpha$  which we compare to the diagonal elements of the inverse FI matrix  $\sqrt{(\mathcal{F}^{-1})_{\alpha\alpha}}$ ,  $\alpha \in \{d, c, p\}$ . We summarize the overall results in Fig. 3. Panel (a) provides the global results in tabular form, while panel (b) presents the results for the ensemble of scenes with  $p_{\text{ref}} = 0.3$ , along with a comparison to the corresponding CRB.

Our experiment demonstrates highly accurate and sensitive multiparameter estimation across a wide range of scene configurations, demonstrating respectively 2 to 4

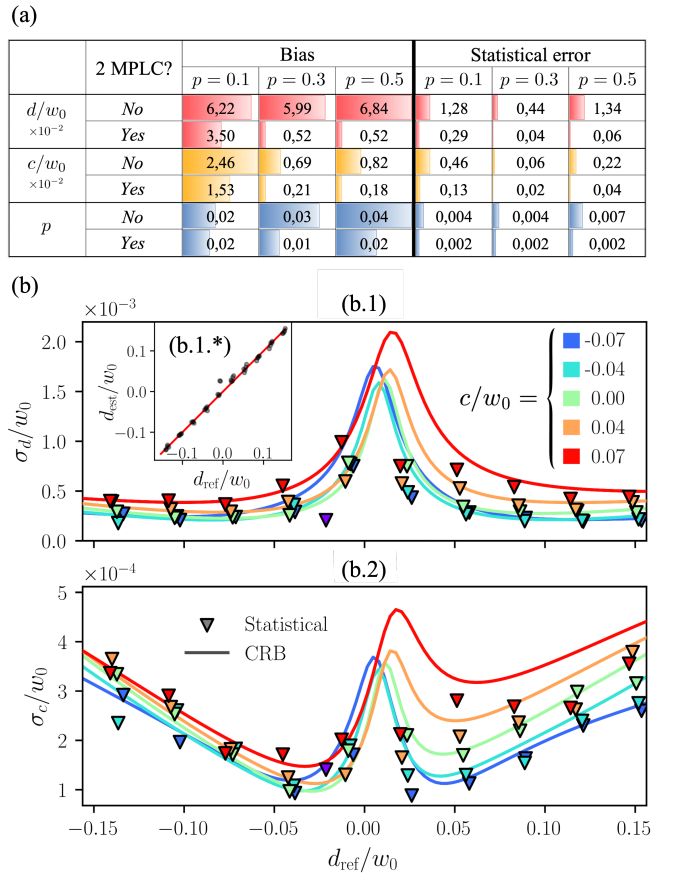


FIG. 3. Multiparameter estimation results on experimental data. Photon flux of  $N = 10^{11}$  over 0.1 ms. (a) Parameter-wise bias and sensitivity for  $d$ ,  $c$ , and  $p$ . For each scene, the bias and sensitivity are computed from the ensemble of time-bin estimates, then averaged over all scenes. Results are grouped by brightness imbalance, and the table also specifies whether the dual-MPLC configuration was used. (b) Detailed results for the case  $p = 0.3$ . (b.1) Statistical errors  $\sigma_d$  and (b.2)  $\sigma_c$ , obtained for each scene from the variability of the time-bin estimates of the separation  $d$  and centroid  $c$ . Errors are shown as functions of the reference parameters  $d_{\text{ref}}$  and  $c_{\text{ref}}$  (see colors legend). Solid lines represent the Cramér—Rao bounds computed from the experimental noise. (b.1.\*)) Mean estimate of separation  $d_{\text{est}}$  versus reference distances  $d_{\text{ref}}$ . The red line denotes unbiased estimation.

orders of magnitude below the Rayleigh limit performances, enabled by the dual-MPLC setup. More specifically, in the dual-MPLC configuration, the achieved bias on the distance (see Fig. 3(b.1.\*)) and centroid is on the order of one hundredth of the beam waist  $w_0$ , while the intensity imbalance is estimated with a one percent precision. The sensitivity on the separation measurement, quantified as the statistical error, reaches approximately  $10^{-3}$  of the waist. As demonstrated in Fig. 3(b.1) and (b.2), the statistical errors closely approach the Cramér—Rao bounds computed from the experimental noise, both for separation and centroid estimation, demonstrating the efficiency of our estimator.

In contrast, performances in terms of bias deteriorate significantly when the second MPLC is omitted, primarily due to an unexpected degeneracy between  $-d$  and  $d$ . In terms of sensitivity, there is also nearly an order of magnitude loss for both  $d$  and  $c$ . These results demonstrate the capacity of our approach to perform accurate and precise multiparameter estimation without prior knowledge of the scene configuration, and highlight the crucial role of the second MPLC in resolving ambiguities and increase precision.

Importantly the precision achieved is orders of magnitude below the diffraction limit, even though we can benefit from the slightly different sources with 99% visibility. In the next section we explore the ideal case of indistinguishable sources to asses the performance of our setup in this scenario.

### C. Results with indistinguishable sources

Depending on practical applications, it may be necessary to resolve two truly indistinguishable sources, in particular when no prior information is available about the sources. To evaluate how the setup would perform under such conditions, we generate data based on the calibration data from a single source. By summing the signals corresponding to two different positions, we reconstruct scenes similar to those analyzed previously, while ensuring source indistinguishability (see supplementary materials). The emulated scenes have separations up to  $0.3w_0$  and only positive  $d$  values, as the problem becomes rigorously symmetrical. The same estimation procedures are then applied, and the results are presented in Figure 4.

It is remarkable that even in this scenario of indistinguishable sources, our dual-MPLC setup enables accurate and precise multiparameter estimation across a wide range of scenes, demonstrating the versatility and applicability of our approach. In terms of bias, performances are comparable to the previous case with slightly different sources, with biases on  $d$  and  $c$  remaining in the  $10^{-2}w_0$  range. One can see that the dual-MPLC configuration significantly reduces the bias of the estimator compared to the single-MPLC case, making the experiment more reliable, a feature that cannot be captured via the CRB analysis.

The obtained sensitivities are degraded compared to the previous case, but still remain in the  $10^{-2}w_0$  range for  $d$  and  $c$  over the full range of parameters. From Fig. 4(b) one can see the efficiency of our estimator for a specific imbalance  $p = 0.3$ . It can be observed that for separations below  $0.1w_0$ , estimators diverge significantly, both in terms of bias and sensitivity, but  $d$  and  $c$  can still be approximated up to  $10^{-1}w_0$  even if  $p$  cannot. Those results are consistent with the diverging CRB for small separation of identical sources. For separation greater than  $0.1w_0$ , the statistical error in separation  $d$  and centroid  $c$  drops below  $10^{-2}w_0$ .

(a)

	2 MPLC?	Bias			Statistical Error		
		$p = 0.1$	$p = 0.3$	$p = 0.5$	$p = 0.1$	$p = 0.3$	$p = 0.5$
$d/w_0 \times 10^{-2}$	No	3,82	2,37	1,96	2,48	1,57	1,38
	Yes	1,96	0,92	0,59	3,08	1,22	0,75
$c/w_0 \times 10^{-2}$	No	4,37	5,58	1,90	2,40	1,82	2,10
	Yes	1,58	1,08	0,14	2,21	1,32	1,10
$p$	No	0,250	0,250	0,090	0,150	0,119	0,118
	Yes	0,120	0,070	0,010	0,122	0,100	0,092

(b)

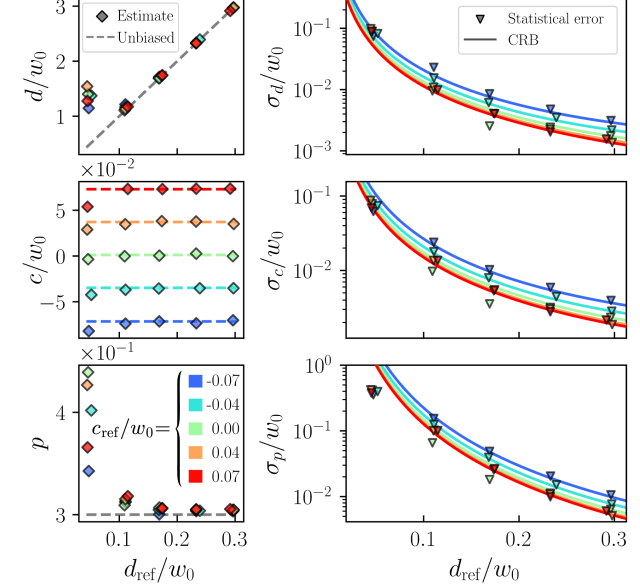


FIG. 4. Estimation results on simulated data for the identical-source case. Photon flux of  $N = 10^{11}$  over 0.1 ms. (a) Same layout as in Fig. 3(a). (b) Specific case of  $p_{\text{ref}} = 0.3$ . Left column: Mean parameter estimates (averaged over all time bins) as functions of the reference parameters  $d_{\text{ref}}$  and  $c_{\text{ref}}$  (see legend). Dashed lines indicate unbiased estimations. Right column: Associated statistical errors, also shown as functions of the reference parameters  $d_{\text{ref}}$  and  $c_{\text{ref}}$ .

## V. CONCLUSION

We have experimentally demonstrated a simultaneous estimation of multiple parameters in the optical domain. In particular, we estimated the separation, centroid, and intensity imbalance for two incoherent point sources using a dual-SPADE architecture in the sub-Rayleigh regime, thereby obtaining superresolution without prior knowledge of the sources. We investigated two complementary classes of scenes: a realistic experimental regime with slightly distinguishable sources (99% overlap), where the highest sensitivities are achieved, with separation uncertainties reaching  $10^{-3}w_0$ , and an idealized regime with indistinguishable sources, where separation and centroid can still be estimated at the  $10^{-2}w_0$  level over a broad parameter range. By jointly addressing these two regimes, our results clarify the practical scope

of multiparameter SPADE measurements for superresolution imaging. Although the experiment was performed in a high-photon-flux regime, the approach can be extended to lower-flux conditions with appropriate detection schemes, bringing it closer to some practical applications such as astronomical imaging. Furthermore, the method is not restricted to two sources and can be straightforwardly generalized to three or more incoherent emitters, with the addition of sources primarily increasing the number of parameters to be jointly estimated.

## ACKNOWLEDGMENTS

This project has received funding from the European Defence Fund (EDF) under grant agreement 101103417 EDF-2021-DIS-RDIS-ADEQUADE. Funded by the European Union. Views and opinions expressed are however those of the author(s) only and do not necessarily reflect those of the European Union or the European Commission. Neither the European Union nor the granting authority can be held responsible for them.

---

[1] C. W. Helstrom, Quantum detection and estimation theory, *Journal of Statistical Physics* **1**, 231 (1969).

[2] A. Holevo, Statistical decision theory for quantum systems, *Journal of Multivariate Analysis* **3**, 337 (1973).

[3] C. Helstrom, Resolution of point sources of light as analyzed by quantum detection theory, *IEEE Transactions on Information Theory* **19**, 389 (1973).

[4] S. L. Braunstein and C. M. Caves, Statistical distance and the geometry of quantum states, *Phys. Rev. Lett.* **72**, 3439 (1994).

[5] M. Barbieri, Optical quantum metrology, *PRX Quantum* **3**, 010202 (2022).

[6] V. Giovannetti, S. Lloyd, and L. Maccone, Advances in quantum metrology, *Nature photonics* **5**, 222 (2011).

[7] M. Gessner, N. Treps, and C. Fabre, Estimation of a parameter encoded in the modal structure of a light beam: a quantum theory, *Optica* **10**, 996 (2023).

[8] G. Sorelli, M. Gessner, N. Treps, and M. Walschaers, Gaussian quantum metrology for mode-encoded parameters, *New Journal of Physics* **26**, 073022 (2024).

[9] N. Rayleigh, XXXI. Investigations in optics, with special reference to the spectroscope, *The London, Edinburgh, and Dublin Philosophical Magazine and Journal of Science* **8**, 261 (1879).

[10] E. Abbe, Beiträge zur theorie des mikroskops und der mikroskopischen wahrnehmung, *Archiv für mikroskopische Anatomie* **9**, 413 (1873).

[11] C. M. Sparrow, On spectroscopic resolving power, *Astrophysical Journal*, vol. 44, p. 76 **44**, 76 (1916).

[12] M. Shahram and P. Milanfar, Statistical and information-theoretic analysis of resolution in imaging, *IEEE Transactions on Information Theory* **52**, 3411 (2006).

[13] M. Tsang, R. Nair, and X.-M. Lu, Quantum theory of superresolution for two incoherent optical point sources, *Phys. Rev. X* **6**, 031033 (2016).

[14] C. Rouvière, D. Barral, A. Grateau, I. Karuseichyk, G. Sorelli, M. Walschaers, and N. Treps, Ultra-sensitive separation estimation of optical sources, *Optica* **11**, 166 (2024).

[15] M. Paúr, B. Stoklasa, Z. Hradil, L. L. Sánchez-Soto, and J. Rehacek, Achieving the ultimate optical resolution, *Optica* **3**, 1144 (2016).

[16] Z. S. Tang, K. Durak, and A. Ling, Fault-tolerant and finite-error localization for point emitters within the diffraction limit, *Opt. Express* **24**, 22004 (2016).

[17] F. Yang, A. Tashchilina, E. S. Moiseev, C. Simon, and A. I. Lvovsky, Far-field linear optical superresolution via heterodyne detection in a higher-order local oscillator mode, *Optica* **3**, 1148 (2016).

[18] W.-K. Tham, H. Ferretti, and A. M. Steinberg, Beating rayleigh's curse by imaging using phase information, *Phys. Rev. Lett.* **118**, 070801 (2017).

[19] Y. Zhou, J. Yang, J. D. Hassett, S. M. H. Rafsanjani, M. Mirhosseini, A. N. Vamivakas, A. N. Jordan, Z. Shi, and R. W. Boyd, Quantum-limited estimation of the axial separation of two incoherent point sources, *Optica* **6**, 534 (2019).

[20] F. Grenapin, D. Paneru, A. D'Errico, V. Grillo, G. Leuchs, and E. Karimi, Superresolution enhancement in biphoton spatial-mode demultiplexing, *Phys. Rev. Appl.* **20**, 024077 (2023).

[21] L. Santamaria, F. Sgobba, and C. Lupo, Single-photon sub-rayleigh precision measurements of a pair of incoherent sources of unequal intensity, *Optica Quantum* **2**, 46 (2024).

[22] J. Řeháček, Z. Hradil, B. Stoklasa, M. Paúr, J. Grover, A. Krzic, and L. L. Sánchez-Soto, Multiparameter quantum metrology of incoherent point sources: Towards realistic superresolution, *Phys. Rev. A* **96**, 062107 (2017).

[23] J. Řeháček, Z. Hradil, D. Koutný, J. Grover, A. Krzic, and L. L. Sánchez-Soto, Optimal measurements for quantum spatial superresolution, *Phys. Rev. A* **98**, 012103 (2018).

[24] J. Liu, H. Yuan, X.-M. Lu, and X. Wang, Quantum fisher information matrix and multiparameter estimation, *Journal of Physics A: Mathematical and Theoretical* **53**, 023001 (2019).

[25] R. Demkowicz-Dobrzański, W. Górecki, and M. Gută, Multi-parameter estimation beyond quantum fisher information, *Journal of Physics A: Mathematical and Theoretical* **53**, 363001 (2020).

[26] A. Boeschoten, G. Sorelli, M. Gessner, C. Fabre, and N. Treps, Estimation of multiple parameters encoded in the modal structure of light, *arXiv preprint arXiv:2505.16435* (2025).

[27] V. Delaubert, N. Treps, C. C. Harb, P. K. Lam, and H.-A. Bachor, Quantum measurements of spatial conjugate variables: displacement and tilt of a gaussian beam, *Opt. Lett.* **31**, 1537 (2006).

[28] M. R. Grace, Z. Dutton, A. Ashok, and S. Guha, Approaching quantum-limited imaging resolution without prior knowledge of the object location, *J. Opt. Soc. Am. A* **37**, 1288 (2020).

[29] M. R. Grace and S. Guha, Identifying objects at the quantum limit for superresolution imaging, *Phys. Rev. Lett.* **129**, 180502 (2022).

[30] K. K. Lee, C. N. Gagatsos, S. Guha, and A. Ashok, Quantum-inspired multi-parameter adaptive bayesian estimation for sensing and imaging, *IEEE Journal of Selected Topics in Signal Processing* **17**, 491 (2023).

[31] A. Sajjad, M. R. Grace, and S. Guha, Quantum limits of parameter estimation in long-baseline imaging, *Phys. Rev. Res.* **6**, 013212 (2024).

[32] J. Frank, A. Duplinskiy, K. Bearne, and A. I. Lvovsky, Passive superresolution imaging of incoherent objects, *Optica* **10**, 1147 (2023).

[33] A. Duplinskiy, J. Frank, K. Bearne, and A. Lvovsky, Tsang's resolution enhancement method for imaging with focused illumination, *Light: Science & Applications* **14**, 159 (2025).

[34] X.-J. Tan, L. Qi, L. Chen, A. J. Danner, P. Kanchanawong, and M. Tsang, Quantum-inspired superresolution for incoherent imaging, *Optica* **10**, 1189 (2023).

[35] M. Parniak, S. Borówka, K. Boroszko, W. Wasilewski, K. Banaszek, and R. Demkowicz-Dobrzański, Beating the rayleigh limit using two-photon interference, *Phys. Rev. Lett.* **121**, 250503 (2018).

[36] J. S. Wallis, D. R. Gozzard, A. M. Frost, J. J. Collier, N. Maron, and B. P. Dix-Matthews, Spatial mode demultiplexing for super-resolved source parameter estimation, *Optics Express* **33**, 34651 (2025).

[37] V. Ansari, B. Brecht, J. Gil-Lopez, J. M. Donohue, J. Řeháček, Z. c. v. Hradil, L. L. Sánchez-Soto, and C. Silberhorn, Achieving the ultimate quantum timing resolution, *PRX Quantum* **2**, 010301 (2021).

[38] J.-F. Morizur, L. Nicholls, P. Jian, S. Armstrong, N. Treps, B. Hage, M. Hsu, W. Bowen, J. Janousek, and H.-A. Bachor, Programmable unitary spatial mode manipulation, *J. Opt. Soc. Am. A* **27**, 2524 (2010).